

A Novel Diamine Adduct of Zinc Bis(2-thenoyl-trifluoroacetate) as a Promising Precursor for MOCVD of Zinc Oxide Films

Graziella Malandrino,^{*,†} Manuela Blandino,[†] Laura M. S. Perdicaro,[†] Ignazio L. Fragalà,^{*,†} Patrizia Rossi,[‡] and Paolo Dapporto[‡]

Dipartimento di Scienze Chimiche, Università di Catania, and INSTM, Udr Catania, Viale A. Doria 6, I-95125 Catania, Italy, and Dipartimento di Energetica, "S. Stecco" Università di Firenze, Via Santa Marta 3, I-50139 Firenze, Italy

Received July 13, 2005

A novel diamine (*N,N,N',N'*-tetramethyletilendiamine) adduct of zinc bis(2-thenoyl-trifluoroacetate) has been synthesized in a single-step reaction. Single-crystal X-ray diffraction studies of Zn(tta)₂·tmeda provide evidence of a mononuclear structure with a six-coordinated zinc ion. The thermal behavior of this adduct points to mass-transport properties suitable for its application to MOCVD processes. This novel compound has been successfully applied as a precursor for the deposition of ZnO films on (100) Si and quartz substrates. The good quality of the deposited films indicates that the adduct is a very attractive precursor for MOCVD applications.

Introduction

Zinc oxide (ZnO) is one of the most promising oxide semiconductor materials because of its good optical, electrical, and piezoelectrical properties. Recently, ZnO has been extensively studied because of its various potential applications, such as gas sensors, photodetectors, light-emitting diodes, and laser systems.¹

ZnO films are required for all these applications. Therefore, a high throughput technique that may represent a potentially scalable process is required for the fabrication of films. These films have been grown using a large variety of techniques, including sublimation,² pulsed-laser deposition (PLD),³ spray pyrolysis (SP),⁴ atomic-layer deposition (ALD),⁵ molecular beam epitaxy (MBE),⁶ chemical-bath deposition (CBD),⁷ sol–gel,⁸ electrodeposition,⁹ oxidation of zinc films,¹⁰ and metal organic chemical vapor deposition

(MOCVD).¹¹ Among them, MOCVD offers several advantages, including the production of high-quality films through a fine-tuning of various processing parameters associated with simpler, less costly equipment, ready scalability, and higher throughput as compared to conventional physical vapor deposition (PVD) techniques.¹²

The success of a MOCVD process depends critically on the availability of volatile, thermally stable precursors that exhibit high and constant vapor pressures to achieve uniform and reproducible film growth.

Previous studies on MOCVD processes of ZnO films have reported the use of liquid dimethyl-Zn¹³ and diethyl-Zn¹⁴ complexes or of the solid acetate,¹⁵ alkoxide,¹⁶ and acetyl-

* To whom correspondence should be addressed. E-mail: gmalandrino@dipchi.unict.it (G.M.), lfragala@dipchi.unict.it (I.L.F.).

[†] Università di Catania.

[‡] Università di Firenze.

- (1) *Materials Today*; June 2004: special issue on ZnO films and nanostructures.
- (2) Tribolate, R.; N'tep, J. M.; Barbe, M.; Lemasson, P.; Mora-Sero, I.; Munoz, V. *J. Cryst. Growth* **1999**, *198/199*, 968–974.
- (3) Fan, X. M.; Lian, J. S.; Guo, Z. X.; Lu, H. J. *Appl. Surf. Sci.* **2005**, *239*, 176–181.
- (4) El Hichou, A.; Addou, M.; Bougrine, A.; Dounia, R.; Ebothe, J.; Troyon, M.; Amrani, M. *Mater. Chem. Phys.* **2004**, *83*, 43–47.
- (5) Ferguson, J. D.; Weimer, A. W.; George, S. M. *J. Vac. Sci. Technol., A* **2005**, *23*, 118–125.
- (6) Izyumskaya, N.; Avrutin, V.; Schoch, W.; Waag, A. *J. Cryst. Growth* **2004**, *269*, 356–361.

- (7) Drici, A.; Djeteli, G.; Tchabgedji, G.; Derouiche, H.; Jondo, K.; Napo, K.; Bernede, J. C.; Ouro-Djobo, S.; Gbagba, M. *Phys. Status Solidi A* **2004**, *201*, 1528–1536.
- (8) Shaoqiang, C.; Zhang, J.; Feng, X.; Xiaohua, W.; Laiqiang, L.; Yanling, S.; Qingsong, X.; Wang, C.; Jianzhong, Z.; Ziqiang, Z. *Appl. Surf. Sci.* **2005**, *241*, 384–391.
- (9) Yoshida, T. *Electrochemistry* **2004**, *72*, 44–48.
- (10) Zhenguo, J.; Shichao, Z.; Chao, W.; Kun, L. *Mater. Sci. Eng., B* **2005**, *117*, 63–66.
- (11) Yang, J. L.; An, S. J.; Park, W. I.; Yi, G.-C.; Choi, W. *Adv. Mater.* **2004**, *16*, 1661–1664.
- (12) Hitchman, M. L.; Jensen, K. F. *Chemical Vapor Deposition: Principles and Applications*; Academic Press: London, 1993.
- (13) Hu, J.; Gordon, R. G. *Mater. Res. Soc. Symp. Proc.* **1991**, *202*, 457.
- (14) Hu, J.; Gordon, R. G. *J. Appl. Phys.* **1992**, *71*, 880–890.
- (15) Jain, S.; Kodas, T. T.; Hampden-Smith, M. *Chem. Vapor. Deposition* **1998**, *4*, 51–59.
- (16) Auld, J.; Houlton, D. J.; Jones, A. C.; Rushworth, S. A.; Malik, M. A.; O'Brien, P.; Critchlow, G. W. *J. Mater. Chem.* **1994**, *4*, 1249–1253.

acetate zinc¹⁷ complexes as precursors. Nevertheless, these precursors have some drawbacks because of their pyrophoric nature, in the case of the dialkyl zinc complexes,¹⁸ and because of the effects of crystallite sizes on the precursor evaporation rate and, hence, on the film growth rate, in the case of solid source.¹⁹ Note that the crystallite sizes may be responsible for changes in evaporation rates in different experiments and, even more importantly, in fluctuations during the same experiment.

Recently, the syntheses of the Zn(hfa)₂(H₂O)₂L adducts with L = diglyme, triglyme, and tetraglyme (H-hfa = 1,1,1,5,5,5-hexafluoro-2,4-pentanedione, diglyme = bis(2-methoxyethyl)ether, triglyme = 2,5,8,11-tetraoxadecane, tetraglyme = 2,5,8,11,14-pentaoxapentadecane) have been reported. Although, these precursors have good thermal stability and volatility, water molecules are present in the coordination sphere independently from the polyether length, i.e., regardless of the number of polyether oxygen atoms, the central metal ion is coordinated by H₂O.²⁰ The most recent study on Zn MOCVD precursors regards the synthesis of diamine adducts of the Zn(hfa)₂ moiety reported by Marks et al.²¹ These precursors are water-free, thermally stable, volatile, and in a liquid state at processing temperatures.

In the present work, we have synthesized and investigated the mass-transport properties of a new water-free zinc adduct, the Zn(tta)₂·tmeda (hta = 2-thenoyltrifluoroacetone, tmeda = N,N,N',N'-tetramethylethylenediamine). The 2-thenoyltrifluoroacetone has been chosen as the anionic ligand because, as for the Cd precursor that is useful for solution routes,²² it could represent a multipurpose single source for ZnO or ZnS phases. The thermogravimetric analyses have shown that this complex is thermally stable and volatile. The functional validation of the Zn(tta)₂·tmeda complex as a MOCVD precursor has been assessed by applying it to the MOCVD of high-quality ZnO films on quartz and Si (100) substrates.

Experimental Section

Reagents. The chemical reagents H-tta and tmeda were purchased from STREM Chemicals. Zn(CH₃COO)₂·2H₂O was purchased from Carlo Erba.

General Procedures. Elemental microanalyses were performed in the Analytical Laboratories of the University of Catania using a Carlo Erba elemental analyzer EA 1108. Thermogravimetric (TG) analyses were performed by using a Mettler Toledo TGA/SDTA 851°. Dynamic thermal investigations were carried out under a purified nitrogen flow (30 sccm) at atmospheric pressure using a 5 °C/min heating rate. The weight of the sample was varied in the range 12–15 mg. The temperature was measured with an accuracy

Table 1. Crystal Data and Refinement Parameters of Complex Zn(tta)₂·tmeda

formula	C ₂₂ H ₂₄ F ₆ N ₂ O ₄ S ₂ Zn
mol wt	623.92
T (K)	298
λ (Å)	0.71069
cryst syst, space group	monoclinic, P2 ₁ /c
a (Å)	11.947(2)
b (Å)	5.368(3)
c (Å)	15.132(3)
β (deg)	92.94(2)
V (Å ³)	2774.6(9)
Z, d _{calc} (g cm ⁻³)	4, 1.494
μ (mm ⁻¹)	1.106
2θ range for data collection (deg)	8.5–64.7
no. of reflns collected/unique data/params	22925/9044 [R(int) = 0.0326] 2663/339
final R indices [I > 2σ(I)]	R1 = 0.0684, wR2 = 0.1970
R indices (all data)	R1 = 0.2028, wR2 = 0.2695

of ±0.1 °C. Isothermal investigations were carried out at 20 Torr. The cylindrical sample boat (12.56 mm² cross sectional area) was filled with ~15 mg of the zinc adduct. The melting points were measured in air with a Koffler microscope. Infrared transmittance spectra were recorded using a Jasco FT/IR-430 spectrometer as Nujol mulls between NaCl plates. The instrumental resolution was 2 cm⁻¹. ¹H and ¹³C NMR spectra were recorded on a Varian Inova 500 spectrometer.

Synthesis. An aqueous solution of Zn(CH₃COO)₂·2H₂O (2.064 g, 9.40 mmol) in 50 mL of H₂O was added to a CH₂Cl₂ solution (40 mL) containing hta (4.177 g, 18.80 mmol) and tmeda (1.418 mL, 9.40 mmol). The resulting solution was vigorously stirred in a separating funnel. The Zn(tta)₂·tmeda, insoluble in the CH₂Cl₂/H₂O mixture, precipitates, and is recovered by adding EtOH (20 mL). The solution was left to crystallize, and the Zn(tta)₂·tmeda crystals were washed with small quantities of pentane, in which the adduct is insoluble. The yield was 75%. Melting point: 128–130 °C at 760 Torr.

Anal. Calcd for C₂₂H₂₄F₆N₂O₄S₂Zn: C, 42.35; H, 3.88; S, 10.28; N, 4.49. Found: C, 42.12; H, 4.01; S, 10.64; N, 4.30.

X-ray Crystallographic Study of Zn(tta)₂·tmeda. A crystal having the dimensions 0.15 × 0.22 × 0.44 mm³ was used for the data collection. Intensity data collection was performed using an Oxford Xcalibur diffractometer with graphite-monochromated Mo Kα radiation (λ = 0.71069 Å), at 298 K.

The cell parameters, the intensity data, and the reduction have been performed using the program package CRYSTALIS, version 1.17.²³ Intensity data were corrected for Lorentz and polarization effects. The absorption correction was made using an analytical method based on faces indexing.

Zn(tta)₂·tmeda crystallizes in the monoclinic system, space group P2₁/c, Z = 4, a = 11.947(2) Å, b = 15.368(3) Å, c = 15.132(3) Å, β = 92.94(2)°.

The structure was solved by direct methods using the SIR97 program,²⁴ and was refined by full-matrix least squares against F² using all data (SHELX97)²⁵ to R1 = 0.0684 for 2663 reflections [I > 2σ(I)]; the number of refined parameters was 339. Anisotropic thermal parameters were used for the non H-atoms. All the hydrogen

- (17) Sato, H.; Minami, T.; Miyata, T.; Takata, S.; Ishii, M. *Thin Solid Films* **1994**, *246*, 65–70.
- (18) Cotton, F. A.; Wilkinson, G.; Murillo, C. A.; Bochmann, M. *Advanced Inorganic Chemistry*, 6th ed.; Wiley-Interscience: New York, 1999.
- (19) Hitchman, M. L.; Shamlian, S. H.; Gilliland, D. C.; Cole-Hamilton, D.; Nash, J. A. P.; Thompson, S. C.; Cook, S. L. *J. Mater. Chem.* **1995**, *5*, 47.
- (20) Gulino, A.; Castelli, F.; Dapporto, P.; Rossi, P.; Fragalà, I. *Chem. Mater.* **2000**, *12*, 548–554.
- (21) Ni, J.; Yan, H.; Wang, A.; Yang, Y.; Stern, C. L.; Metz, A. W.; Shu, J.; Wang, L.; Marks, T. J.; Ireland, J. R.; Kannewurf, C. R. *J. Am. Chem. Soc.* **2005**, *127*, 5613–5624.
- (22) Malandrino, G.; Finocchiaro, S. T.; Rossi, P.; Dapporto, P.; Fragalà, I. L. *Chem. Commun.* **2005**, 5681–5683.

- (23) (a) *CrysAlis CCD*, version 1.171.pre23_10 beta; Oxford Diffraction Ltd.: Oxford, U.K.; release 21.06.2004 CrysAlis171.NET (compiled June 21, 2004, 12:00:08). (b) *CrysAlis RED*, version 1.171.pre23_10 beta; Oxford Diffraction Ltd.: Oxford, U.K.; release 21.06.2004 CrysAlis171.NET (compiled June 21, 2004, 12:00:08).
- (24) Altomare, A.; Casciaro, G.; Giacovazzo, C.; Guagliardi, A.; Burla, M. C.; Polidori, G.; Camalli, M. *J. Appl. Crystallogr.* **1994**, *27*, 435.
- (25) Sheldrick, G. M. *SHELXL-97*; University of Göttingen: Göttingen, Germany, 1997.

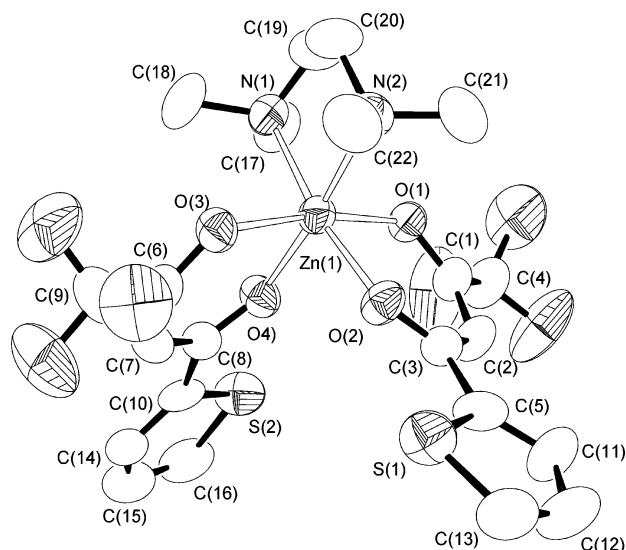


Figure 1. ORTEP view of the compound $\text{Zn}(\text{tta})_2 \cdot \text{tmeda}$.

atoms were introduced in calculated positions, and were refined according to the linked atoms; the overall temperature factor converged to $0.145(5) \text{ \AA}^2$.

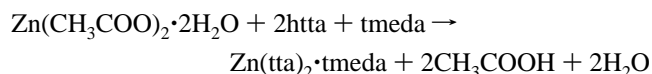
Geometric calculations were performed by PARST97,²⁶ and molecular plots were produced by the program ORTEP3.²⁷ Table 1 reports crystallographic data and structure refinement parameters. In Figure 1 an ORTEP3 drawing of the complex is reported.

MOCVD Experiment and Film Characterization. ZnO films were prepared in a reduced-pressure, horizontal, hot-wall MOCVD reactor from the $\text{Zn}(\text{tta})_2 \cdot \text{tmeda}$ precursor contained in a resistively heated alumina boat. Quartz and Si (100) substrates were used for the depositions. In this study, the precursor evaporation temperature was kept at $170 \text{ }^\circ\text{C}$, whereas the reactor temperature was kept at $650 \text{ }^\circ\text{C}$. Ar (150 sccm) and O_2 (150 sccm) flows were used as carrier and reaction gases, respectively. The mass flows were controlled with an MKS 1160 flowmeter using an MKS 147 electronic control unit. Depositions were carried out for 60 min. The total pressure in the reactor was about 3 Torr.

θ - 2θ X-ray diffraction (XRD) patterns were recorded on a Bruker-AXS D5005 θ - θ X-ray diffractometer, using Cu $K\alpha$ radiation operating at 40 kV and 30 mA. Film-surface morphology was examined using a LEO iridium 1450 scanning electron microscope (SEM). Energy-dispersive X-ray analysis (EDX) spectra were obtained using an IXRF detector.

Results and Discussion

Synthesis. The adduct $\text{Zn}(\text{tta})_2 \cdot \text{tmeda}$ has been prepared through immediate reaction from zinc acetate bihydrate, 2-thenoyltrifluoroacetone, and N,N,N',N' -tetramethylethylenediamine. The synthetic route to the complex is reported in the following scheme



The adduct is soluble in ethanol and acetone, whereas it is insoluble in solvents such as CH_2Cl_2 , H_2O , n -pentane, and n -hexane. The reaction can be easily carried out on open benches, without the need for a controlled atmosphere. The

Table 2. Selected Bond Distances (\AA) and Angles ($^\circ$) for $\text{Zn}(\text{tta})_2 \cdot \text{tmeda}$

Zn(1)–O(1)	2.062(3)	O(1)–Zn(1)–O(2)	86.25(12)
Zn(1)–O(2)	2.078(3)	O(1)–Zn(1)–O(3)	169.55(12)
Zn(1)–O(3)	2.055(3)	O(1)–Zn(1)–O(4)	85.20(12)
Zn(1)–O(4)	2.093(3)	O(1)–Zn(1)–N(1)	89.62(14)
Zn(1)–N(1)	2.177(4)	O(1)–Zn(1)–N(2)	96.90(15)
Zn(1)–N(2)	2.188(4)	O(2)–Zn(1)–O(3)	89.06(12)
		O(2)–Zn(1)–O(4)	95.83(13)
		O(2)–Zn(1)–N(1)	170.34(14)
		O(2)–Zn(1)–N(2)	89.59(15)
		O(3)–Zn(1)–O(4)	85.99(12)
		O(3)–Zn(1)–N(1)	96.37(14)
		O(3)–Zn(1)–N(2)	92.39(15)
		O(4)–Zn(1)–N(1)	92.52(15)
		O(4)–Zn(1)–N(2)	174.32(15)
		N(1)–Zn(1)–N(2)	82.23(16)

present low-cost synthetic procedure gives a water-free and nonhygroscopic adduct. The complex is stable in air, and its melting point is $128\text{--}130 \text{ }^\circ\text{C}$ at 760 Torr. These are important issues for source precursors used for CVD applications for which low-cost chemicals that may be manipulated on open benches are an important objective.

X-ray Crystallographic Study of $\text{Zn}(\text{tta})_2 \cdot \text{tmeda}$. The Zn(1) ion is hexacoordinated; the six donor atoms are four oxygen atoms of two tta anions and two nitrogen atoms of one tmeda molecule (Figure 1). The coordination geometry may be described as distorted octahedral (see Table 2).

All the Zn–O and Zn–N bond distances are in agreement with those retrieved from the Cambridge Structural Database (CSD, version 5.25)²⁸ for zinc complexes having acetylacetonate derivatives and tmeda as ligands. The retrieved ranges are $2.002\text{--}2.161 \text{ \AA}$ (mean value = 2.076 \AA) and $2.086\text{--}2.411 \text{ \AA}$ (mean value = 2.172 \AA) for Zn–O and Zn–N distances, respectively.

The tta anions are characterized by extended conjugation, as shown by the fact that all the atoms of each tta anion, except the fluorine ones, lie on a plane. The maximum deviation from the mean plane featuring O(3) and O(4) as donors is $0.060(8) \text{ \AA}$ for C(9). The second tta ligand appears to be a little bit more distorted with respect to the mean plane (C(4) shows the highest deviation, $0.370(8) \text{ \AA}$). The angle between the two mean planes is $84.57(8)^\circ$.

The tmeda molecule, acting as a chelating ligand, shows a gauche conformation; the dihedral angle N1–C19–C20–N2 has a value of $55.3(7)^\circ$. With regard to the relative disposition of the three ligands, the mean plane defined by the tmeda atoms N1, C19, C20, and N2 forms angles of $78.8(3)$ and $72.1(2)^\circ$ with the mean planes defined by all the non-hydrogen atoms of the two tta anions (with the exception of the fluorine atoms).

In the CSD, we retrieved the complex $\text{Co}(\text{tta})_2 \cdot \text{tmeda}$.²⁹ This complex is quite isomorphous and isostructural with $\text{Zn}(\text{tta})_2 \cdot \text{tmeda}$. The RMS value found superimposing the metal cation as well as the six donor atoms is 0.031 \AA .

Finally, if we consider the plane defined by the metal cation and the CH carbon atoms of the two tta anions, the two thiophene rings lie on opposite sides with respect to it.

(26) Nardelli, M. *Comput. Chem.* **1983**, *7*, 95–98.

(27) Farrugia, L. J. *J. Appl. Crystallogr.* **1997**, *30*, 565.

(28) Allen, F. H. *Acta Crystallogr., Sect. B* **2002**, *58*, 380–388.

(29) Tzavellas, L. C.; Tsiamis, C.; Kavounis, C. A.; Cardin, C. J. *Inorg. Chim. Acta* **1997**, *262*, 53–59.

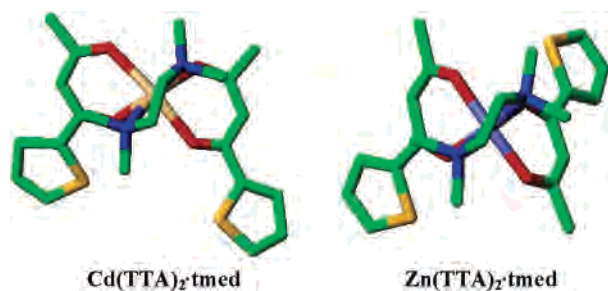


Figure 2. Structure of the $\text{Zn}(\text{tta})_2 \cdot \text{tmeda}$ adduct compared to that of the homologous $\text{Cd}(\text{tta})_2 \cdot \text{tmeda}$.

Table 3. Peaks in the ^1H NMR Spectrum of the $\text{Zn}(\text{tta})_2 \cdot \text{tmeda}$ Adduct

$^1\text{H-NMR}$	δ (ppm)
N-CH_3	2.50
N-CH_2	2.83
CO-CH-CO	6.20
H_b	7.14
H_a, H_c	7.73-7.79

In the crystal lattice, no intermolecular contacts are present. A cis configuration has been instead observed for the $\text{Cd}(\text{tta})_2 \cdot \text{tmeda}$ complex (Figure 2). This difference may be responsible for the completely different behavior in terms of thermal properties of the Zn and Cd homologues, as the $\text{Zn}(\text{tta})_2 \cdot \text{tmeda}$ is highly thermally stable and volatile whereas the $\text{Cd}(\text{tta})_2 \cdot \text{tmeda}$ analogue decomposes, leaving a CdF_2 residue.²²

Physicochemical and Mass-Transport Properties of $\text{Zn}(\text{tta})_2 \cdot \text{tmeda}$. The Fourier transform infrared (FT-IR) spectrum of the present $\text{Zn}(\text{tta})_2 \cdot \text{tmeda}$ shows no band at 3600 cm^{-1} , thus providing evidence of no coordinated water molecules and hence a complete saturation of the zinc center by the tmeda nitrogen atoms. Peaks at 1616 cm^{-1} , 1596 cm^{-1} ($\text{C}=\text{O}$ stretching vibrations), and 1536 cm^{-1} ($\text{C}=\text{C}$ stretching vibrations) are typical of the β -diketonate ligand. The other bands, observed at $1300\text{--}1000 \text{ cm}^{-1}$, represent C-N bending and/or stretching of the tmeda ligand overlapped with the C-F and C-S stretchings. In particular, peaks between 1230 and 1030 cm^{-1} are associated with C-N stretching vibrations of the tmeda ligand. Peaks at 2923 , 1460 , and 1377 cm^{-1} are due to the Nujol used to prepare the mull.

The ^1H NMR spectrum (Table 3) of the $\text{Zn}(\text{tta})_2 \cdot \text{tmeda}$ adduct shows a singlet at $\delta = 6.20$ whose integration accounts for the two protons, one for each tta ring. The multiplet at $\delta = 7.14$ represents the resonance of the H_b protons of the thiophene ring, whereas the multiplets between $\delta = 7.73$ and 7.79 are associated with resonances of the H_a and H_c protons (see Scheme 1). In addition, multiplets at $\delta = 2.50$ and 2.83 represent resonances of the six and four protons, respectively, of the tmeda methyl and methylene groups.

Scheme 1

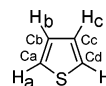
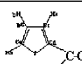
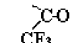


Table 4. Peaks in the ^{13}C NMR Spectrum of the $\text{Zn}(\text{tta})_2 \cdot \text{tmeda}$ Adduct

$^{13}\text{C-NMR}$	δ (ppm)
N-CH_3	46.65 (sing)
N-CH_2	56.29 (sing)
$\text{C}_a, \text{C}_b, \text{C}_c$	128 ÷ 133
C_d	146.34
CO-CH-CO	89.60 (sing)
$-\text{CF}_3$	119.15 (quad)
	183.46 (sing)
	172.06 (quad)

The ^{13}C NMR spectrum (Table 4) of the $\text{Zn}(\text{tta})_2 \cdot \text{tmeda}$ adduct shows a singlet at $\delta = 46.65$ and a singlet at $\delta = 56.29$ that are associated with carbons of the methyl and methylene groups, respectively, of the tmeda. A singlet at $\delta = 89.60$ represents the resonance of the C in the α position of the tta ring, whereas the singlets between $\delta = 128$ and 133 represent the resonances of the C_a , C_b , and C_c carbons of the thiophene ring. The singlet at $\delta = 146.34$ is associated with the resonance of C_d , whereas the quartet at $\delta = 119.15$ ($^1J = 286.2 \text{ Hz}$) is associated with the resonance of carbons of the $-\text{CF}_3$ groups. Finally, the singlet at $\delta = 183.46$ and the quartet at $\delta = 172.06$ ($^2J = 31.4 \text{ Hz}$) represent resonances of the carbonic carbons linked, respectively, to the thiophene ring and to the $-\text{CF}_3$ group.

The thermal behavior of the present Zn precursor has been investigated by dynamic and static thermogravimetric (TG) analyses. The TG profile recorded at atmospheric pressure and isothermal curves measured at 20 Torr in a purified nitrogen flow are reported in Figures 3 and 4, respectively. The thermogravimetric first derivative (DTG) (Figure 3) consists of a single peak, thus indicating that the precursor evaporates quantitatively in the $200\text{--}320 \text{ }^\circ\text{C}$ range, with about 5% residue left at $450 \text{ }^\circ\text{C}$. It can be concluded that the $\text{Zn}(\text{tta})_2 \cdot \text{tmeda}$ precursor shows a clean vaporization with a low residue, as required for MOCVD applications.

Isothermogravimetric curves have been evaluated in the $150\text{--}190 \text{ }^\circ\text{C}$ interval (Figure 4) under a reduced pressure (20 Torr) of pure N_2 . In this temperature range, the adduct is melted; thus the linearity of vaporization for all the investigated temperatures indicates that this compound may

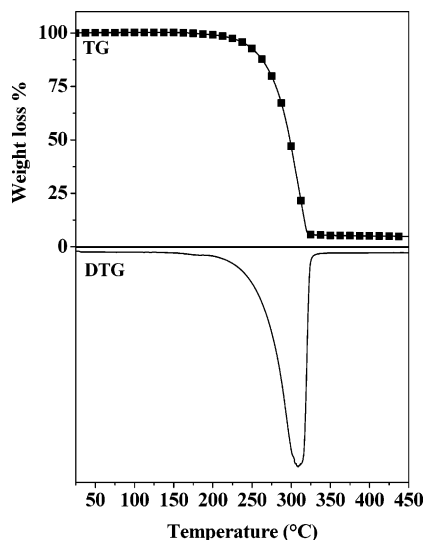


Figure 3. TG/DTG profiles of the $\text{Zn}(\text{tta})_2 \cdot \text{tmeda}$ adduct under a N_2 flow in the 25–450 °C temperature range.

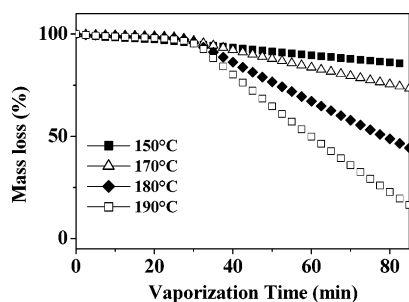


Figure 4. Weight changes with time for vaporization of $\text{Zn}(\text{tta})_2 \cdot \text{tmeda}$ at various temperatures and a reduced pressure of 20 Torr under a N_2 flow.

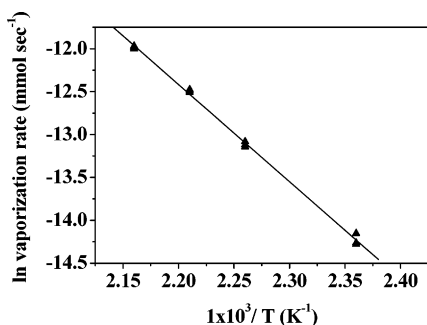


Figure 5. Arrhenius plot for the evaporation of $\text{Zn}(\text{tta})_2 \cdot \text{tmeda}$.

be used as a liquid precursor under processing conditions. For each investigated temperature, the vaporization rate remains constant during the 60 min experiment.

Figure 5 shows the Arrhenius relationship obtained by plotting the vaporization rate as a function of the reciprocal temperature. A linear relationship is evident, as expected for vaporization processes without any side decomposition. The apparent molar enthalpies of the vaporization process (calculated from the slope of the Arrhenius plot) have been evaluated to be $90 \pm 1 \text{ kJ mol}^{-1}$.

All these investigations clearly indicate that the $\text{Zn}(\text{tta})_2 \cdot \text{tmeda}$ compound is thermally stable and volatile, and therefore it is expected to be a good precursor for the deposition of zinc-containing films.

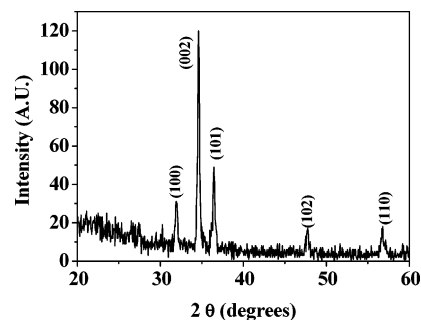


Figure 6. XRD pattern of a ZnO film deposited on a quartz substrate from a $\text{Zn}(\text{tta})_2 \cdot \text{tmeda}$ precursor at 650 °C.

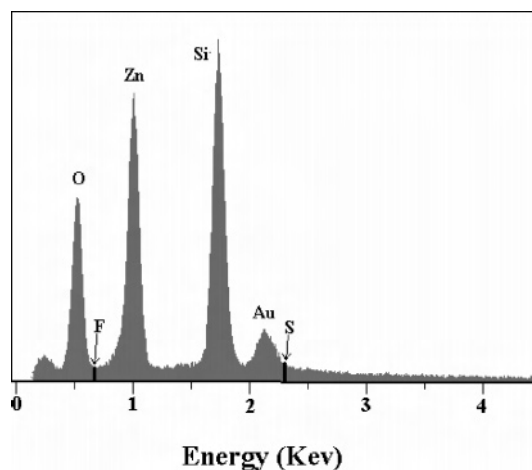


Figure 7. EDX spectrum of a ZnO film deposited at 650 °C.

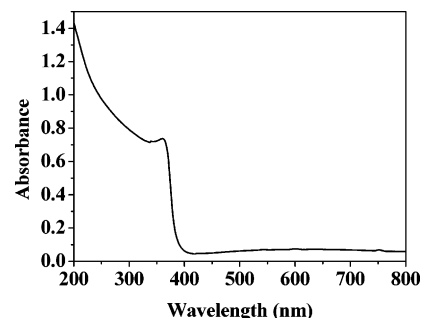


Figure 8. UV-visible absorption spectrum of a ZnO film deposited at 650 °C.

MOCVD Depositions from the $\text{Zn}(\text{tta})_2 \cdot \text{tmeda}$ Precursor. The final assessment of a potential precursor for MOCVD processes may only be obtained by applying it to the fabrication of films containing the specific metallic center. In the present case, the $\text{Zn}(\text{tta})_2 \cdot \text{tmeda}$ precursor has been validated through its successful application to the fabrication of ZnO films. Preliminary experiments have been made on Si (100) and quartz substrates at 650 °C, while maintaining the precursor temperature at 170 °C. Note that at this temperature, the zinc adduct is molten, thus representing a liquid precursor. Films deposited are uniform with smooth surfaces, and grazing incidence XRD patterns (Figure 6) exhibit peaks at 2θ of 31.90, 34.55, 36.40, 47.75, and 56.75°. These peaks may be associated with the 100, 002, 101, 102, and 110 reflections, respectively, of the hexagonal wurtzite ZnO phase.³⁰

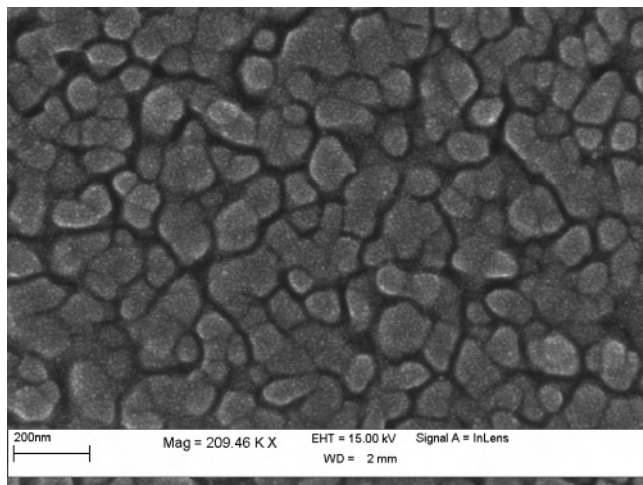


Figure 9. SEM image of a ZnO film deposited at 650 °C.

The compositional purity of the ZnO films has been confirmed by energy-dispersive X-ray analysis (EDX). The EDX spectrum, reported in Figure 7, shows the presence of the ZnL peaks at about 1.010 keV. The peak at 1.730 keV is due to the Si K α peak of the quartz substrates, whereas the peak at 2.120 keV is due to the Au sputtered on the sample. In addition, note that the use of the windowless EDX detector allowed for the detection of the O K α peak at 0.560 keV and the exclusion of any S and/or F contamination, thus ruling out any sulfide and/or fluoride phase. In this context, it is worth noting that dry oxygen is used as the reaction gas, and therefore no fluoride phases form during deposition.

The UV–visible absorption spectrum of a ZnO film grown on quartz at 650 °C is shown in Figure 8. This spectrum shows that the ZnO film is highly transparent in the visible region with nearly 90% transmission between 400 and 800

(30) ICDD No. 36–1451 in *Powder Diffraction File*; International Centre of Diffraction Data: Newton Square, PA.

nm. The absorbance in the UV region at about 370 nm can be related to the band-to-band transition.

Finally, the surface morphology of this ZnO film has been investigated by scanning electron microscopy. The sample (Figure 9) presents a very uniform morphology, with coalesced grains of about 100 nm. The surface of each grain is highly nanostructured, and domains smaller than 10 nm are visible on the grain surface.

Conclusions

The present synthetic strategy has proven to be an efficient route for the preparation of a thermally stable and volatile zinc adduct from commercially available products. The novel Zn(tta)₂•tmeda represents, to the best of our knowledge, the first reported example of adducts of zinc with tta β -diketonate. The dynamic and static TG measurements indicate that this adduct possesses mass-transport properties suitable for MOCVD applications. In addition, the Zn(tta)₂•tmeda may be used in the molten phase, thus representing a liquid precursor under processing conditions, as isothermogravimetric measurements indicate the adduct is also thermally stable in the liquid phase. In fact, MOCVD experiments on quartz and (100) Si substrates yielded high-quality ZnO films in terms of phase purity, morphology, and transparency. These data clearly point to the efficacy and great potential of this precursor for depositing ZnO nanostructured films.

Acknowledgment. The authors thank the MIUR for the financial support. CRIST (Centro Interdipartimentale di Cristallografia Strutturale) University of Florence is gratefully acknowledged.

Supporting Information Available: Crystallographic information files (CIF). This material is available free of charge via the Internet at <http://pubs.acs.org>.

IC051175I